1990ApJ...360..184K

THE ASTROPHYSICAL JOURNAL, 360:184–196, 1990 September 1
© 1990. The American Astronomical Society. All rights reserved. Printed in U.S.A.

W30 REVEALED: SEPARATION AND ANALYSIS OF THERMAL AND NONTHERMAL EMISSION IN A GALACTIC COMPLEX

NAMIR E. KASSIM[1] and KURT W. WEILER
Center for Advanced Space Sensing, Naval Research Laboratory
Received 1989 August 10; accepted 1990 March 5

ABSTRACT

We present new VLA observations of the W30 Galactic complex at 90 and 20 cm. By combining these data with existing radio continuum and recombination line observations extending from wavelengths of 10 m to 3 cm, we are able to do the following:

i) We can improve estimates of the spectra and physical properties of H II regions in the complex. For thermal sources which are optically thick at 90 cm, we derive improved emission measures and filling factors, and for those which are optically thin, we set new upper limits to their emission measures.

ii) We can derive improved estimates of the spectrum and physical properties of the supernova remnant (SNR) G8.7–0.1 associated with the W30 complex. Our 90 cm observations show that the nonthermal emission from the SNR is much larger than previously realized. The newly determined spectral index $\alpha = -0.5$ is typical of shell-type SNRs. Relating G8.7–0.1 to H II regions in the W30 complex yields an improved distance estimate for the SNR of $\sim 6 \pm 1$ kpc. At this distance G8.7−0.1 is one of the largest known Galactic SNRs, with a physical size of ~ 80 pc, and certainly one of the most distant, low–surface brightness SNRs known in the Milky Way.

iii) We can show that the low-frequency turnover in the spectrum of G8.7−0.1 is due to absorption by localized thermal gas associated with one or more of the H II regions near the W30 complex and does not require absorption by a distributed ionized component of the ISM.

iv) We can show that, with this new distance and larger extent, G8.7−0.1 may be associated with the very young pulsar, PSR 1800−21.

Subject headings: nebulae: H II regions — nebulae: individual (W30) — nebulae: supernova remnants — pulsars

I. INTRODUCTION

At radio continuum centimeter wavelengths, the W30 complex appears as a large ($\sim 1°$), roughly circular region of extended emission with a number of superposed, smaller diameter ($\leq 20'$) sources (Reich *et al.* 1984; Altenhoff *et al.* 1978; Handa *et al.* 1988). CO observations also show molecular gas associated with the region (Blitz, Fich, and Stark 1982). Most of the discrete sources have been identified as H II regions, but the nature of the remaining sources of radio emission in the complex, particularly the extended component, has remained unclear. Odegard (1986*a*), using 57.5 MHz observations made with the Clark Lake TPT synthesis array (Erickson, Mahoney, and Erb 1982), was able to establish the northern part of the extended emission as being nonthermal and on this basis identified a new Galactic supernova remnant (SNR), G8.7−0.1. However, at 57.5 MHz much of the southwestern part of the complex appears in absorption, confirming the presence in this area of foreground H II regions (at 57.5 MHz thermal sources, because they have become optically thick, appear in absorption against any nonthermal sources or against the Galactic background if they are relatively close. They became undetectable if they are distant [Kassim 1987, 1988*a*; Odegard 1986*a*, *b*]) but limiting his ability to determine the exact distribution of thermal and nonthermal gas in W30.

Higher frequency, single-dish surveys (Altenhoff *et al.* 1978; Reich *et al.* 1984; Handa *et al.* 1988) of the Galactic plane are also unable to clarify the nature of the mixed emission from W30. While they are not affected by absorption, the H II regions in the complex become strong emitters, the steeper spectrum nonthermal components become relatively weaker, and, as for all single-dish measurements, the strong Galactic background emission limits the dynamic range and the ability to distinguish individual structures.

By using new, high-resolution VLA[2] observations at 90 and 20 cm (resolution $\sim 3'.5$ and $1'.4$, respectively) and combining these with other results available in the literature, we are able to better define the nature and physical properties of both the thermal and nonthermal components of W30. These intermediate wavelengths (particularly 90 cm) allow us to better separate the nonthermal SNR G8.7−0.1 and the thermal H II regions than is possible at shorter centimeter wavelengths while not yet being hindered by the thermal absorption which affects the meter-wavelength results. We are able to confirm the identification of G8.7−0.1 as a Galactic SNR, to better establish its extent, and to estimate more accurately its physical properties. Our 90 cm observations also allow us to distinguish between the optically thick and optically thin H II regions in W30 and improved estimates of their physical properties.

Because it is possible to relate several of the H II regions, whose distances are known, to G8.7−0.1, we are able to obtain a new distance estimate of $\sim 6 \pm 1$ kpc and add it to the very short list of SNRs which have distances established indepen-

[1] ONT/NRL Cooperative Research Fellow.

[2] The VLA is a facility of the National Radio Astronomy Observatory operated by Associative Universities, Inc., under a cooperative agreement with the National Science Foundation.

© American Astronomical Society • Provided by the NASA Astrophysics Data System

1990ApJ...360..184K

dent of Σ–D assumptions. Not only does the close spatial association of G8.7−0.1 with the H II regions suggest that it may be an example of a causal relation between supernovae and star forming regions in Galactic H II/Molecular cloud complexes, but the new distance for G8.7−0.1 greatly strengthens the possibility of an association of the SNR with the young pulsar PSR 1800−21, whose age and distance estimates are very similar.

II. OBSERVATIONS

The W30 complex was observed with the VLA in two 50 MHz bands centered at 1480.7 MHz and 1536.2 MHz (λ-20 cm) with a 12 antenna subarray and in two 3 MHz bands centered at 327.5 MHz and 333.0 MHz (λ-90 cm) with a 15 antenna subarray during 1987 March. The telescope was in the "D" configuration (maximum baseline ~1 km) yielding elliptical synthesized beams with full width at half-maximum (FWHM) of 4′.1 × 2′.8 at position angle 11° for 90 cm and 1′.8 × 0′.9 at position angle −19° for 20 cm. The total integration time for each map was approximately 1 hr, consisting of six 10 minute snapshots spread over an 8 hr period to maximize the available uv coverage.

Calibration at 20 cm used single 20 minute observations of primary calibrators 3C 286 and 3C 48, defined to have flux densities of 14.51 and 15.76 Jy, respectively, to determine the variable flux density of the secondary calibrator 1741−038 at the epoch of observation. Then, observations for ~10 minutes each hour of 1741−038, which is compact and has a well-determined position, were used to calibrate the phase and flux density for the 20 cm data set. At 90 cm, no secondary calibrators were used, and flux density and phase calibration were based directly on observations of 3C 286, 3C 380, and 3C 48 which were defined to have flux densities of 29, 45, and 47 Jy, respectively. Standard computer programs were used to interpolate the gain and phase of the instrument between calibrator observations. These procedures are normal for the VLA and are thought to provide a flux density calibration which is consistent to a few percent with possible systematic errors of up to ~5% at both wavelengths. For a more detailed description of the VLA see Napier, Thompson, and Ekers (1983).

The shortest array spacings at 20 and 90 cm were ~200λ and ~30λ, respectively. This means that sources larger than ~3′ at 20 cm and ~20′ at 90 cm may be undersampled and have their flux densities underestimated by greater than ~10%. The individual maps, after calibration, correction, and inspection for quality, were added to produce a single map for each observing band. These "dirty" maps were then CLEANed and restored with elliptical Gaussians. The final maps, after correction for primary beam attenuation, are shown in Figures 1 (90 cm) and 2 (20 cm). The measured rms levels are ~0.07 Jy beam^{-1} on the 90 cm map and ~0.035 Jy beam^{-1} on the 20 cm map.

III. RESULTS

a) New VLA Maps

On all maps, the known H II regions are assigned letter designations A–G and marked with plus (+) signs. These regions have been identified by higher frequency recombination line studies and lower frequency continuum observations which are summarized below (§§ III*b*, *c*). Their positions are listed in Table 1. On our 90 cm map (Fig. 1), the position of PSR 1800−21, which was not detected, is marked with a star

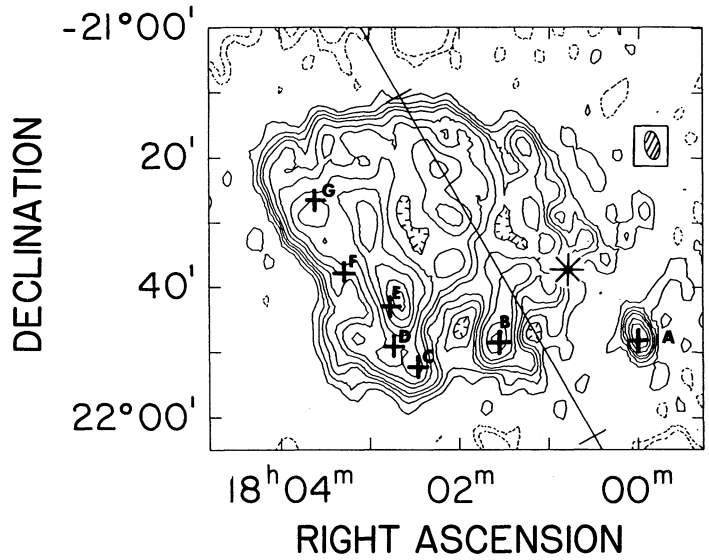

FIG. 1.—Contour map, corrected for primary beam attenuation, of the W30 complex at 90 cm wavelength (330 MHz). The half-power beamwidth of 4′.1 × 2′.8 at P.A. 11° is shown in the upper right-hand corner. Contour levels are at (−0.50, −0.25, 0.25, 0.50, 0.75, 1.00, 1.50, 2.00, 3.00,..., 7.00) × 0.5 Jy beam^{-1}, with the peak brightness in the map being 3.76 Jy beam^{-1} at the position $\alpha = 18^h02^m38^s$, $\delta = -21°42'00''$. The brightness temperature scale is 1 Jy beam^{-1} ≈ 302 K. The position of PSR 1800−21 is marked with a star (*), and the positions of known H II regions are marked with plus (+) signs and letter designations A–G. The Galactic plane is shown with tick marks at $l = 8°$ and $l = 9°$, with Galactic latitude increasing to the northeast.

(*). The broadly extended emission not associated with any of the known H II regions is nonthermal so that it is apparently part of the W30 SNR, G8.7−0.1 (see § IV*b*). Several of the known H II regions (A–D) appear as peaks on the 90 cm map superposed above the extended emission, while two of these (F and G) show little evidence for emission above the back-

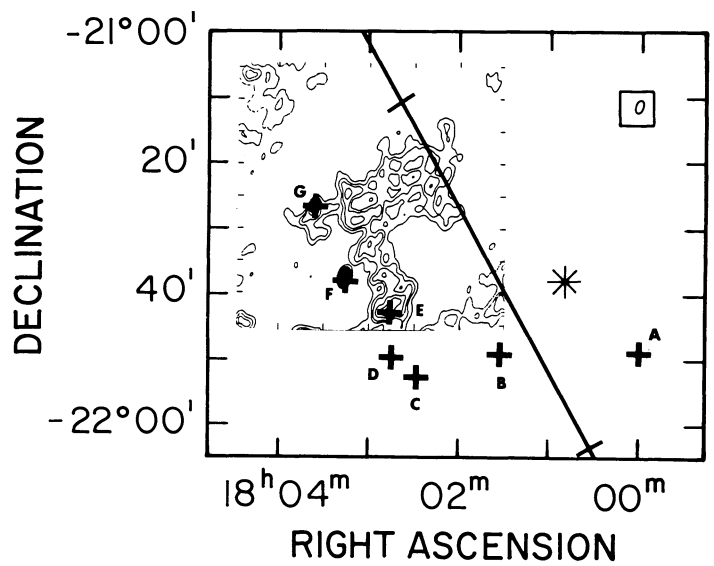

FIG. 2.—Contour map, corrected for primary beam attentuation, of the W30 complex at 20 cm wavelength (1508 MHz). The half-power beamwidth of 1′.8 × 0′.9 at P.A.−−19° is shown in the upper right-hand corner. Contour levels are at (−3, −2, −1, 0.25, 0.50, 0.75, 1.25, 1.75, 2.25, 3.00, 4.00) × 0.1 Jy beam^{-1} with the peak brightness in the map being 0.39 Jy beam^{-1} for the source (*F*) at $\alpha = 18^h03^m16^s$, $\delta = -21°37'40''$. The brightness temperature scale is 1 Jy beam^{-1} ≈ 105 K. Source and Galactic coordinate markings as in Fig. 1.

© American Astronomical Society • Provided by the NASA Astrophysics Data System

1990ApJ...360..184K

TABLE 1

POSITIONS OF KNOWN H II REGIONS IN THE W30 COMPLEX[a]

Source[b]	G Number	R.A. (1950)	Decl. (1950)
A	G8.14+0.23	$18^h00^m00^s$	−21°48′06″
B	G8.31−0.09	18 01 33	−21 48 45
C	G8.36−0.30	18 02 28	−21 52 21
D	G8.44−0.33	18 02 44	−21 49 13
E	G8.53−0.29	18 02 46	−21 42 59
F	G8.67−0.36	18 03 19	−21 37 50
G	G8.86−0.33	18 03 37	−21 26 50

[a] Positions for sources B, C, D, and E are obtained from the 6 cm map (Fig. 3) by Altenhoff *et al.* 1978 (FWHP = 2′.7), for sources A and F, from the 7 mm observations by Wood *et al.* 1988 (FWHP = 0′.7), and for source G, from our 20 cm VLA map (FWHP = 1′.8 × 0′.9, Fig. 2).

[b] See Fig. 1.

ground. The position of H II region E is slightly offset from a peak on the 90 cm map, suggesting this maximum may be a blend of thermal emission from the H II region and a separate peak in the nonthermal extended emission.

Because the primary beam of the VLA 25 m dishes is 35′ (FWHM) at 20 cm, our Figure 2 provides information only about the northeastern part of the W30 complex. The compact H II regions F and G are unresolved but clearly detected. Source E is also detected in our 20 cm map, and it is clearly extended. However, because the primary beam correction for it is very high (≥10 times), the poorer signal-to-noise and unavoidable errors in the primary beam model mean our 20 cm flux density estimate for it is unreliable. A new 20 cm VLA map of W30 by Braun, Goss, and Lyne (1989) (FWHP 1′.0 × 0′.5) is centered further south and shows an extended region of emission near R.A. = 18^h01^m, decl. = −21°38′.5, which appears to be a detection of the southwestern part of G8.7−0.1. Their map also provides flux density and size limit estimates for Sources A and B (see Tables 2 and 4), both of which appear to be marginally resolved.

The VLA results for H II regions A–G, the pulsar PSR 1800−21, and the SNR G8.7−0.1 are summarized in Table 2. To obtain integrated flux densities from our 90 cm map for these sources we have assumed that sources A, B, C, F, and G are unresolved and that Gaussian models adequately describe sources D and E. This is a reasonable assumption, since sources A and B are only slightly resolved on the higher resolution 20 cm Braun, Goss, and Lyne (1989) map while sources C, F, and G are apparently unresolved on all available maps (see also § III*b* and Fig. 3). Flux density errors arise mainly in the uncertainty of determining the local background for each source, and the estimates given in Table 2 reflect this. In all cases, these errors exceed those expected due to random noise. Note that the background contribution for our 90 and 20 cm observation is only due to the extended emission of G8.7−0.1 since, unlike on single-dish maps, the much more extended emission from the Galactic background is resolved out by the VLA.

The integrated flux density at 90 cm for G8.7−0.1 listed in Table 2 has been corrected for contributions from the superposed H II regions B–G. Separation of the thermal from nonthermal components is somewhat involved and is discussed in detail in § IV. PSR 1800−21, whose position is marked with a star (*) in Figure 1, was not detected at 90 cm, but an upper limit to its flux density can be established and is listed in Table 2. The relationship between PSR 1800−21 and G8.7−0.1 is discussed further in § VII and in Kassim and Weiler (1990).

From our 20 cm VLA map (Fig. 2) we have obtained flux densities for the unresolved H II regions F and G. For H II regions A and B we list flux densities obtained from the 20 cm VLA D-array map by Braun, Goss, and Lyne (1989) (corrected by our own estimates of the primary beam attenuation in their map) and from the 20 cm VLA B-array survey source list by Garwood *et al.* (1988) (HPBW ~ 4″), respectively. Exami-

TABLE 2

NEW VLA RESULTS FOR SOURCES IN THE W30 COMPLEX

	90 CENTIMETERS		20 CENTIMETERS	
SOURCE	Peak Brightness[a,b] (Jy beam^{-1})	Integrated Flux Density (Jy)	Peak Brightness[a,b] (Jy beam^{-1})	Integrated Flux Density (Jy)
A	1.54 ± 0.15	Point[c]	≥1.151[d]	Point[c]
B	0.88 ± 0.25	Point[c]	≥0.270[d]	≥0.751[d]
C	1.18 ± 0.50	Point[c]	...	...
D	1.04 ± 0.50	6.22 ± 2.99	...	...
E	1.50 ± 1.00	8.10 ± 5.40	...	...
F	≤0.150	Point[c]	0.389 ± 0.035	Point[c]
G	≤0.150	Point[c]	0.32 ± 0.035	Point[c]
PSR 1800−21	≤0.250	Point[c]	0.015[e]	Point[c]
G8.7−0.1	4.06 ± 0.15	129 ± 11[f]	...	...

[a] After background subtraction.

[b] The factor for conversion to kelvins is 1 Jy beam^{-1} ≈ 302 K at 90 cm, 1 Jy beam^{-1} ≈ 105 K at 20 cm.

[c] For an unresolved, "point" source, the integrated flux density in Jy is equal to the peak brightness in Jy beam^{-1}.

[d] The brightness and 20 cm flux densities for sources A and B are estimated from the 20 cm VLA map of Braun, Goss, and Lyne 1989 and the 20 cm VLA B-array survey source list by Garwood *et al.* 1988, respectively. These are lower limits, since both sources show slight evidence of extended emission on the VLA D-array Braun, Goss, and Lyne 1989 map.

[e] From Braun, Goss, and Lyne 1989.

[f] We measure a total flux density of 146 Jy for G8.7−0.1 plus the contribution from the superposed H II regions B–G. In § IV*b* we estimate the net thermal contribution to be 17 Jy, leaving 129 Jy due to the SNR alone.

© American Astronomical Society • Provided by the NASA Astrophysics Data System

1990ApJ...360..184K

TABLE 3

RECOMBINATION LINE DETECTIONS IN THE W30 COMPLEX

A. H110α OBSERVATIONS (DOWNES ET AL. 1980)

Source (1)	R.A. (1950) (2)	Decl (1950) (3)	Continuum Temperature T_C(K) (4)	Line Temperature T_L(K) (5)	Velocity (km s^{-1}) (6)	Emission Measure[a] EM (cm^{-6} pc) (7)	T_e[a,b] (K) (8)
A	$18^h00^m00^s$	−21°48′18″	6.9	0.44	22.0	4.7×10^5	6500
C	18 02 28	−21 52 21	1.8	0.11	36.0	2.1×10^4	7300
F	18 03 17	−21 37 55	2.6	0.09	40.0	3.4×10^5	11000

B. H76α OBSERVATIONS (WINK, WILSON, AND BIEGING 1983)

Source	R.A. (1950)	Decl (1950)	Line to Continuum Ratio T_L/T_C	Velocity (km s^{-1})	T_e (K)
A	$18^h00^m00^s$	−21°48′17″	0.222 ± 0.010	22.1 ± 0.6	5600 ± 400
F	18 03 18	−21 37 55	0.170 ± 0.015	42.7 ± 1.1	6700 ± 900

C. 3 cm (H85α, H87α, H88α) OBSERVATIONS (LOCKMAN 1989)

Source	R.A. (1950)	Decl. (1950)	Line Temperature T_L (mK)	Velocity (km s^{-1})	FWHM (km s^{-1})
A	$18^h00^m00^s$	−21°48′18″	146 ± 6.5	20.6 ± 0.6	25.4 ± 1.3
B	18 01 33	−21 48 45	48 ± 4.1	46.8 ± 0.7	15.6 ± 1.6
C	18 02 28	−21 52 21	31 ± 3.2	36.8 ± 1.6	32.2 ± 3.8
D	18 02 44	−21 49 13	44 ± 5.0	38.0 ± 0.8	14.7 ± 1.9
E	18 02 46	−21 42 59	34 ± 4.4	39.2 ± 0.9	14.0 ± 2.1
F	18 03 17	−21 37 55	54 ± 3.9	41.9 ± 1.0	27.9 ± 2.3
G	18 03 36	−21 26 41	21 ± 2.2	31.0 ± 1.5	28.9 ± 3.5

[a] Assumes that the sources are optically thin and in local thermodynamic equilibrium (LTE).
[b] Errors in the electron temperatures are estimated by Downes *et al.* 1980 to be ±2500 K.

nation of the Braun, Goss, and Lyne (1989) map and flux densities listed by Garwood *et al.* (1988) indicate that sources A and B may be slightly resolved so that the 20 cm flux densities listed in Table 2 should be considered as lower limits. The 20 cm flux density for PSR 1800−21 is taken from Braun, Goss, and Lyne (1989).

b) W30: Higher Frequency, Single-Dish Results

i) *Single-Dish Radio Recombination Lines*

Sources A–G correspond to positions from which hydrogen recombination lines have been detected (Lockman 1989; Downes *et al.* 1980; Wink, Wilson, and Bieging 1983) which identifies them as H II regions, and Table 3 summarizes the available recombination line data. The most complete data are line brightness temperature (T_L) and velocities obtained from Lockman (1989). Downes *et al.* (1980) obtain estimates for the emission measure (EM) and electron temperature (T_e) from H110α observations by assuming that the sources are optically thin and in local thermodynamic equilibrium (LTE), but these estimates of EM are lower limits for sources unresolved by the 2′.7 beam of the Effelsberg 100 m telescope or for sources with significant clumping. The estimates for T_e by Wink, Wilson, and Bieging (1983) from the Effelsberg H76α recombination line survey are thought to be less sensitive to non–LTE effects but, in any case, they do not differ significantly from those determined from the H110α line observations. This supports the conclusion that LTE electron temperatures are frequently close to actual T_e (see, e.g., Seaton 1980; Shaver 1980; Wilson (1980). We discuss constraints on the physical properties and distances to the H II regions based on the recombination line results in §§ IV*a* and V*a*, respectively.

ii) *Single-Dish Continuum Results*

Probably the best picture of the large-scale structure surrounding W30 is from the 6 cm Galactic survey with 2′.7 resolution made with the Effelsburg 100 m telescope (Altenhoff *et al.* 1978). We reproduce their map of the area in Figure 3 and again indicate the thermal sources A–G with plus signs (+). The position of the pulsar PSR 1800−21 is again marked with a star. This same general structure is also seen on single-dish maps made at 3 cm (resolution 3′.0; Handa *et al.* 1988) and at 11 cm (resolution 4′.3; Reich *et al.* 1984) although with somewhat less detail and with, as expected, the flat spectrum thermal emission becoming relatively more prominent at the shorter wavelengths.

Table 4 summarizes the single-dish continuum flux density and size information available from the literature for the known H II regions at higher frequencies. (The more complicated estimation of the integrated flux density for G8.7−0.1 from the single-dish maps has been deferred to § IV*b*, where we derive a detailed spectrum of the SNR). As with our 90 cm VLA data, the flux densities listed in Table 4 have been obtained by assuming that sources A, B, C, F, and G are unresolved, and sources D and E can be fit with Gaussian models.

Experience shows that the principle source of error in determining flux densities on these single-dish surveys is the difficulty in estimating the local background level. In the W30

© American Astronomical Society • Provided by the NASA Astrophysics Data System

1990ApJ...360..184K

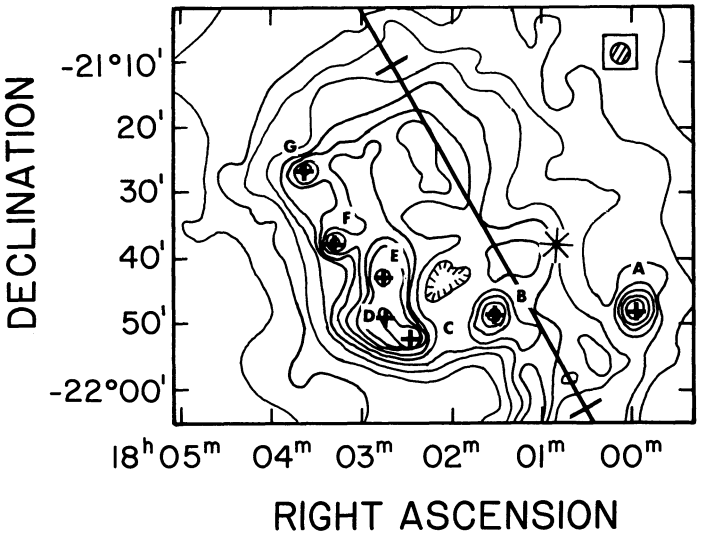

FIG. 3.—An enlarged portion of the 6 cm Galactic survey (resolution 2'.7) by Altenhoff *et al.* (1978) showing the large-scale structures surrounding the W30 complex. The half-power beamwidth is 2'.7 and is shown in the upper right-hand corner. Source and Galactic coordinate markings are as in Fig. 1.

complex, there is background both from the extended emission of G8.7−0.1 and the Galactic background radiation. In our estimates, we have attempted to allow for the maximum background determination uncertainty so that our error estimates are conservative.

The last column of Table 4 provides an estimate of the spectral index for each of the thermal sources A–G from our 90 cm observations (Table 2) and the 3 cm integrated flux densities of Handa *et al.* (1988). Sources A, F and G are known to be compact H II regions (sizes $< \sim 1'$; see col. [5] of Table 4) so that their positive 90 cm–3 cm spectral indices are consistent with them having already become optically thick at 90 cm. On the other hand, the known to be extended thermal sources D and E are still optically thin at 90 cm and have typical thermal spectral indices. These results imply that sources B and C with $\alpha = -0.14$ and $\alpha = -0.16$, respectively, although unresolved on all available maps, are still optically thin at 90 cm and thus are probably not dominated by compact ($\ll 1'$) structure. We discuss the physical properties of the individual H II regions A–G quantitatively in § IV*a* where their spectra throughout the radio regime are derived.

c) W30: Lower Frequency Results

The 57.5 MHz map of Odegard (1986*a*) (resolution 7'.2 × 9'.7 FWHP) is shown in Figure 4. The areas of absorption seen in Figure 4 are due to extended, foreground H II regions, and comparison with Figures 1 and 3 shows that sources C and D absorb strongly. (Comparison of Fig. 4 with our 90 cm map [Fig. 2] shows that the 57.5 MHz emission is from a much smaller region than the 90 cm [330 MHz] emission, mainly due to the absorption by extended foreground H II regions C and D.) Source D is known to be extended (Table 4, col. [5]), and source C is also apparently not very compact, since it has an optically thin 90 cm–3 cm spectral index (Table 4, col. [6]), consistent with its being a prominent 57.5 MHz absorber. Furthermore, source B, which is apparently still optically thin at 90 cm (90 cm–3 cm spectral index $\alpha = -0.14$; Table 4) and therefore likely to be extended, may be absorbing the southwestern portion of G8.7−0.1 in Figure 4. At such a low frequency as 57.5 MHz, any emission must be nonthermal so that, based on his map and comparison with the 11 cm Effelsburg map of this region (Reich *et al.* 1984), Odegard (1986*a*) identified this emission as a new Galactic SNR, G8.7−0.1. However, only the southern and western "tongues" of nonthermal emission on Odegard's map hint at the much greater extent of G8.7−0.1 seen more clearly in our 90 cm map.

A 30.9 MHz map of the W30 region appears in the Clark Lake Galactic Plane survey (Kassim 1988*b*), where the synthesized beamwidth is 13'.9 × 18'.5 (FWHP). After correction for registration differences caused by ionospheric refraction,[3] the correspondence between emission and absorption features in Figure 4 and the 30.9 MHz map is good, although a number of discrete features have become blended on the 30.9 MHz map due to the larger synthesized beam. Kassim's 30.9 MHz SNR candidate G9.1+0.1 (Kassim 1988*a*, *b*) is seen to correspond to G8.7−0.1 and falls within his expected position uncertainty. As at 57.5 MHz, foreground thermal gas absorbs emission from the southern and western parts of G8.7−0.1.

Although the resolution is too poor at these low frequencies to separate individual sources and components and the H II regions have gone into absorption, we can obtain integrated flux density values for G8.7−0.1, and these are discussed in § IV*b*.

IV. DETERMINATION AND ANALYSIS OF SOURCE SPECTRA

As we have shown above, the numerous thermal sources in the W30 complex can be separated from the extended, underlying (SNR and Galactic background) emission by their compact morphology (Fig. 3), available recombination line data (Table 3), very low frequency absorption (Figs. 4 and 5),

[3] An ionospheric refraction correction of +20' in declination should be applied to Kassim's 30.9 MHz map for correct registration with the 57.5 MHz map (Fig. 4). Such shifts are common at long wavelengths for sources at low declinations, but to first order they do not appear to result in significant distortion of the brightness distribution. See Erickson (1983) and Kassim (1988*b*) for a further discussion of the effects of such refraction on low frequency continuum maps.

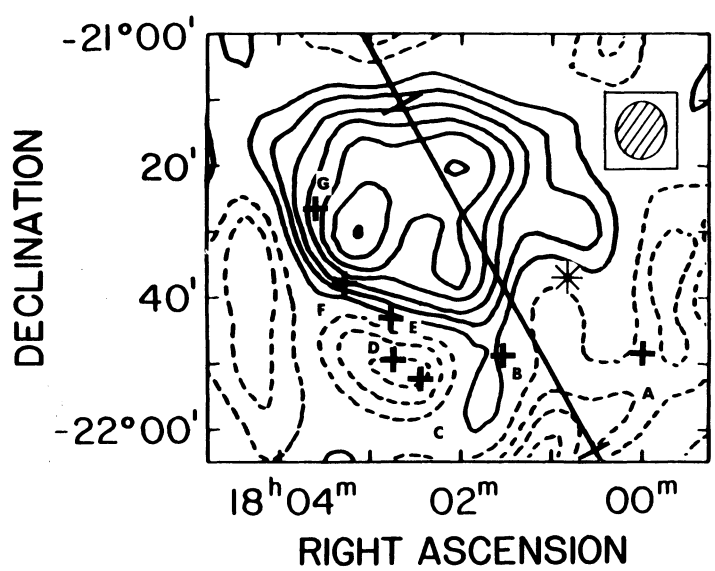

FIG. 4.—57.5 MHz Clark Lake Radio Observatory (CLRO) map of Odegard (1986*a*). The half-power beamwidth of 7'.2 × 9'.7 (EW) is shown in the upper right-hand corner. Source and Galactic coordinate markings are as in Fig. 1. The brightness temperature scale is 1 Jy beam^{-1} ≈ 1470 K.

© American Astronomical Society • Provided by the NASA Astrophysics Data System

1990ApJ...360..184K

TABLE 4

HIGH-FREQUENCY ($\nu > 1$ GHz) SINGLE-DISH CONTINUUM RESULTS FOR THERMAL SOURCES IN THE W30 COMPLEX

Source (1)	Wavelength[a] (cm) (2)	Peak Brightness[b] T_p(K) (3)	Integrated Flux Density[c] S(Jy) (4)	Size[d] (arcmin) (5)	90 cm–3 cm Spectral Index[e] $\alpha(S \propto \nu^{+\alpha})$ (6)
A.....	11	10.48	4.19 ± 0.10	≤1.0 × 0.5[f]	...
	6	9.26	4.63 ± 0.05	...	...
	3	1.50	4.20 ± 0.14	...	+0.36
B.....	11	1.75	0.70 ± 0.08	≤1.0 × 0.5[f]	...
	6	0.90	0.45 ± 0.10	...	...
	3	0.20	0.55 ± 0.14	...	−0.14
C.....	11	2.30	0.92 ± 0.44	≤2.7 × 2.7	...
	6	1.40	0.70 ± 0.40	...	...
	3	0.25	0.69 ± 0.42	...	−0.16
D.....	11	2.75	4.36 ± 1.60	8.5 × 8.5	...
	6	1.60	7.48 ± 2.16	...	...
	3	0.20	4.52 ± 2.24	...	−0.15
E.....	11	2.75	3.94 ± 1.40	9.2 × 7.1	...
	6	1.25	6.04 ± 2.40	...	...
	3	0.20	4.06 ± 2.04	...	−0.20
F.....	11	2.00	0.80 ± 0.40	≤1.8 × 0.9	...
	6	2.70	1.35 ± 0.30	...	...
	3	0.45	1.26 ± 0.28	...	≥ +0.63
G.....	11	1.10	0.44 ± 0.12	≤1.8 × 0.9	...
	6	1.10	0.55 ± 0.10	...	...
	3	0.15	0.42 ± 0.28	...	≥ +0.30

[a] 11 cm observations from Reich *et al.* 1984 (1 K ≈ 0.4 Jy beam^{-1}, FWHP = 4′.3); 6 cm observations from Altenhoff *et al.* 1978 (1 K ≈ 0.5 Jy beam^{-1}, FWHP = 2′.7); 3 cm observations from Handa *et al.* 1988 (1 K ≈ 2.8 Jy beam^{-1}, FWHP = 3′.0).

[b] After background subtraction.

[c] Flux densities are obtained by assuming all sources are unresolved on the single-dish maps except sources G and H, which were estimated by a Gaussian fitting procedure. Errors are estimated from the uncertainty in determining the local background levels.

[d] Sizes for sources A and B from the 20 cm VLA D-array map by Braun, Goss, and Lyne 1989 (FWHP 1′.0 × 0′.5), for C, D, and E, from the 6 cm map by Altenhoff *et al.* 1978 (FWHP = 2′.7), and for F and G, from our 20 cm VLA map (FWHP = 1′.8 × 0′.9).

[e] For the 90 cm flux densities, see Table 2.

[f] Sources A and B appear only marginally resolved on the 20 cm VLA D-array map by Braun, Goss, and Lyne 1989 (FWHP 1′.0 × 0′.5) so that we can accept them as unresolved on the single-dish maps and our 90 cm map (Fig. 1).

and 90 cm–3 cm spectral index (Table 4, col. [6]). There is also enough information available to derive a spectrum for each source and to constrain its physical properties.

a) Thermal Sources A–G

Kassim *et al.* (1989, hereafter K89) have shown that flux density measurements of thermal sources which are optically thick at low frequencies (≤330 MHz) and optically thin at higher frequencies (≥2695 MHz), combined with electron temperatures derived from recombination line observations, can be used to significantly improve estimates of H II region emission measures and filling factors. The assumptions inherent in this method have been discussed in detail in K89 and are not repeated here.

For the W30 H II regions A, F, and G which appear to be optically thick at 90 cm, the electron temperatures[4] (T_e[K]; Table 3A, col. [8]) determined by recombination line observations can be combined with our measured 90 cm flux densities ($S_{90\ \mathrm{cm}}$[Jy]) to obtain an estimate of the effective source size ($\Omega_{90\ \mathrm{cm}}$[rad]) (from K89; eq. [5], ν = 327 MHz):

$$\Omega_{90\ \mathrm{cm}} = 3.01 \times 10^{-4} T_e^{-1} S_{90\ \mathrm{cm}} \,. \quad (1)$$

This effective source size, when combined with the optically thin flux density at 3 cm ($S_{3\ \mathrm{cm}}$[Jy]; Table 5, col. [3]) and the assumed T_e yields an improved value of the emission measure (EM) (from K89; eq. [7]):

$$\mathrm{EM} = 1.65 T_e^{1.35} S_{3\ \mathrm{cm}} S_{90\ \mathrm{cm}}^{-1}\ \mathrm{cm}^{-6}\ \mathrm{pc} \,. \quad (2)$$

A filling factor can then be calculated as the ratio of the effective source size $\Omega_{90\ \mathrm{cm}}$ to the apparent source size Ω_{map} if one is available. As discussed in K89, if the H II regions consist of high-density clumps embedded in a more widely distributed, lower density, ionized component, our derived emission measures, while generally an order of magnitude higher than any previous estimates available from centimeter wavelength single-dish observations, are still only lower limits.

The method used in K89 depends on electron temperatures determined from recombination line measurements and these

[4] We use values of T_e from the H76α survey of Wink, Wilson, and Bieging (1983) when available, otherwise from the H110α survey of Downes *et al.* (1980), since the former are thought to be less sensitive to non–LTE effects.

© American Astronomical Society • Provided by the NASA Astrophysics Data System

1990ApJ...360..184K

are not available for source G. No electron temperatures can be derived from Lockman's deep survey (Lockman 1989) since no line to continuum temperature ratio is available and source G is too faint to have been detected in the H110α (Downes *et al.* 1980) and H76α (Wink, Wilson, and Bieging 1983) surveys. However, we can make a useful estimate of T_e for source G from using the results of § V*a* (below) in which we constrain the H II regions near the W30 complex to be at a distance of 6 ± 1 kpc (corresponding to a galactocentric distance $D_{GC} = 4$ kpc) together with a model of H II region electron temperatures as a function of galactocentric distance. Wink, Wilson, and Bieging (1983) find $T_e = 4800 + 270 D_{GC}$ (from a least-squares fit for 84 H II regions and using D_{GC} for the Sun of 10 kpc and the standard Schmidt Galactic rotation model) which gives $T_e =$ 5900 K ($\pm \sim 1000$ K) for source G. Therefore we assume an electron temperature of 5900 K for source G and recognize that our derived emission measure and filling factor involve this further assumption. Quantitatively, if T_e is in error by 40% ($\sim 2\ \sigma$), the value of the emission measure changes by $1.4^{1.35}$ or $\sim 60\%$. While this may seem large, it still provides an estimate of the emission measure where none was previously available.

The results for the 90 cm optically thick H II regions A, F, and G are collected in Table 5. Columns (2), (4), and (5) repeat the needed values from previous tables for convenience, column (3) is calculated by fitting an $\alpha = -0.1$ (H II region optically thin) spectrum to the measured centimeter wavelength flux densities listed in Table 4, and columns (6)–(8) contain, respectively, the improved emission measures, effective sizes, and filling factors calculated from equations (1) and (2). These parameters completely determine the radio spectra for these three sources.

The radio flux density of a spherical H II region in the LTE, homogeneous nebula approximation (Hjellming, Andrews, and Sejnowski 1969) is given by (see K89, eq. [1]):

$$S = 3.07 \times 10^{-2} T_e \nu^2 \Omega (1 - e^{-\tau}) , \quad (3)$$

where S is the integrated flux density in Jy, T_e is the electron temperature in Kelvin, ν is the observing frequency in MHz, Ω is the solid angle in steradians subtended by the source, and τ is the optical depth. At radio wavelengths, τ is given (Mezger and Henderson 1967) approximately by (see K89, eq. [2]):

$$\tau \sim 1.643 \times 10^5 \nu^{-2.1} \mathrm{EM}\, T_e^{-1.35} , \quad (4)$$

where EM is the emission measure in cm^{-6} pc, defined as

$$\mathrm{EM} = \int_L n_e^2\, dl , \quad (5)$$

with n_e the thermal electron density in cm^{-3} and l the path length in parsecs along a line of sight L through the source.

Using equations (3) and (4), along with the measured and derived parameters listed in Table 5, the spectra for sources A, F, and G are calculated. These are plotted, along with all known flux density measurements, as the solid lines in Figure 5*a*–5*c*. The agreement between the calculated spectra and the measured flux densities indicates that our estimates of the physical properties of H II regions A, F, and G are quite reasonable. Note also that the derived emission measures (Table 5) suggest that sources F and G may be ultracompact (UC) H II regions.[5] Source A is certainly compact (< 1′; see Table 4) but the large filling factor (~ 1) indicates it does not have ultracompact structure.

H II regions B–E appear to be optically thin at 90 cm so that the available flux density measurements can be fitted with a thermal emission spectrum of $\alpha = -0.1$. This is shown together with the available flux density measurements in Figures 6*a*–6*d*. While no estimate of the filling factor or the effective source size ($\Omega_{90\ \mathrm{cm}}$) is possible for these optically thin regions, assuming an electron temperature of 6300 K allows us to place an upper limit on the EM by requiring $\tau \leq 0.1$ in equation (4). These upper limits are listed in Table 5.

b) G8.7−0.1: The W30 SNR

The extended nonthermal emission from G8.7−0.1 is well determined by our 90 cm observations. As can be seen (Fig. 1),

[5] Wood and Churchwell (1989) define ultracompact H II regions as small, photoionized nebulae with diameters ≤ 0.1 pc, electron densities $\geq 10^4$ cm^{-3}, and emission measures $\geq 10^7$ cm^{-6} pc. Only our sources F and G may satisfy these conditions (see Table 5).

TABLE 5

MEASURED AND DERIVED PARAMETERS FOR H II REGIONS IN THE W30 COMPLEX

	Measured Parameters				Derived Parameters[a]		
Source (1)	$S_{90\ \mathrm{cm}}$[b] (Jy) (2)	$S_{3\ \mathrm{cm}}$[c] (Jy) (3)	T_e[d] (K) (4)	Ω_{map}[e] (sr) (5)	EM (cm^{-6} pc) (6)	$\Omega_{90\ \mathrm{cm}}$ (sr) (7)	Filling Factor $\Omega_{90\ \mathrm{cm}}/\Omega_{\mathrm{map}}$ (8)
A	1.54	4.1	5600	6.9×10^{-8}	5.0×10^5	8.2×10^{-8}	~ 1
B	0.88	0.5	5900	$\geq 4.2 \times 10^{-8}$	$\leq 1.5 \times 10^4$	...	...
C	1.18	0.7	7300	$\leq 6.2 \times 10^{-7}$	$\leq 1.9 \times 10^4$	...	...
D	6.22	0.9	5900	6.1×10^{-6}	$\leq 1.5 \times 10^4$	...	...
E	8.10	5.1	5900	5.5×10^{-6}	$\leq 1.5 \times 10^4$	...	...
F	≤ 0.150	1.1	6700	$\leq 4.2 \times 10^{-8}$	$\geq 1.7 \times 10^6$	6.7×10^{-9}	0.16
G	≤ 0.150	0.4	5900	$\leq 1.4 \times 10^{-7}$	$\geq 6.0 \times 10^5$	7.6×10^{-9}	0.06

[a] The new estimates are obtained from eqs. (1) and (2) for H II regions A, F, and G, which are optically thick at 90 cm. For sources B, C, D, and E, which are optically thin at 90 cm, only an upper limit to the emission measure can be derived by assuming $\tau_{90\ \mathrm{cm}} \leq 0.1$.

[b] From Table 2, col. (3).

[c] Calculated by fitting an $\alpha = -0.1$ (optically thin) thermal spectrum to the measured centimeter wavelength flux densities listed in Table 4.

[d] $T_e = 5900$ K is assumed (see § IV*a*) except for sources A, C, and F, which are taken from Table 3A, col. (8) (H76α values for sources A and F, H110α value for source C).

[e] From Table 4, col. (5).

© American Astronomical Society • Provided by the NASA Astrophysics Data System

1990ApJ...360..184K

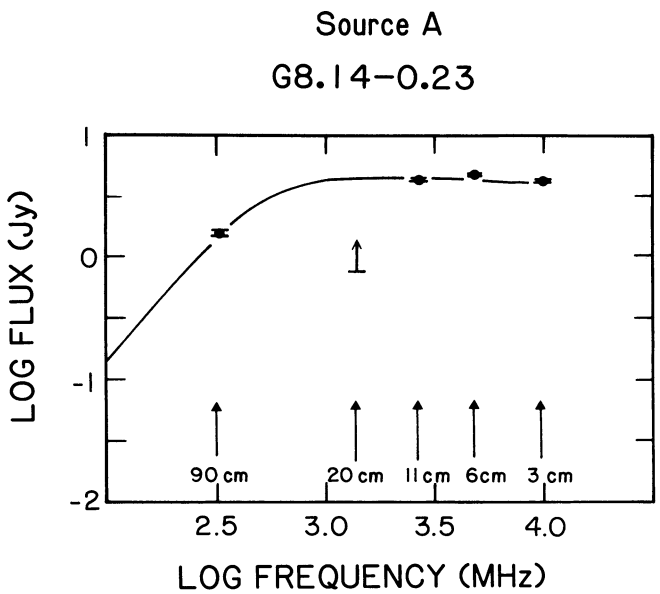

FIG. 5*a*

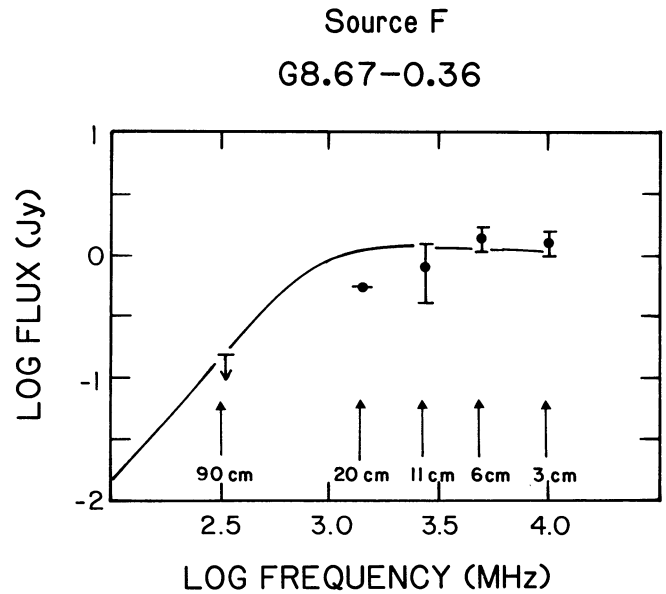

FIG. 5*b*

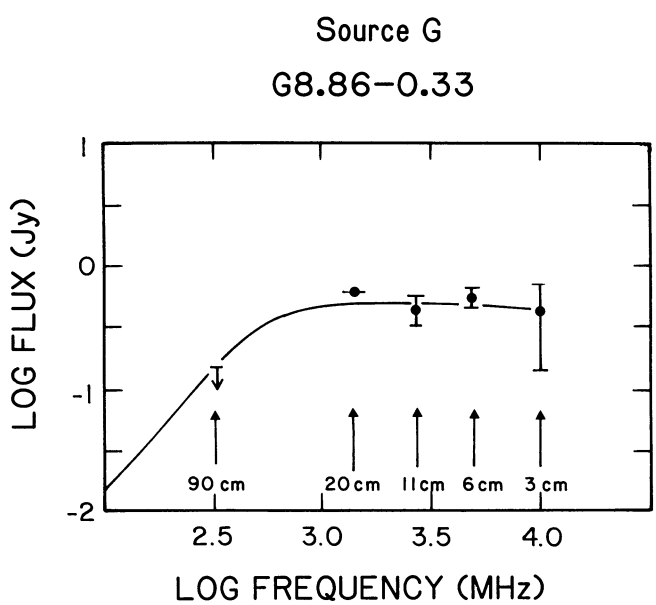

FIG. 5*c*

FIG. 5.—(*a*)–(*c*) Spectra of the H II regions A, F, and G in the W30 complex which are optically thick at 90 cm. The spectra (*solid lines*) are derived from the parameters listed in Table 5 and eqs. (3) and (4) using the method described in K89. The available flux density measurements from Tables 2 and 4 are also plotted.

it is much larger than previously realized since the absorption by foreground H II regions which affects the southwestern part of the complex on lower frequency Clark Lake maps (Fig. 4 and Kassim's 1988*b* 30.9 MHz map) is absent.

In fact, G8.7−0.1 may even be larger than is apparent from our 90 cm map. D-array, VLA observations attenuate structures greater than ~1° in size so that our estimate of the 90 cm flux density may only be a lower limit. Although confused by broad Galactic background emission, the 6 cm, single-dish map of Altenhoff *et al.* (1978) (Fig. 3) suggests that G8.7−0.1 may extend further to the west than is seen in Figure 1. However, since the best available picture of the nonthermal emission from G8.7−0.1 is our 90 cm map, we shall use it to define the most accurate form, size, and flux density available for the SNR.

i) *Spectrum*

As the best approximation possible from the observations available at present, we describe G8.7−0.1 as slightly elliptical and centered at R.A. (1950) = 18^h02^m, decl. (1950) = −21°34′ for all frequencies. For flux density integration, since it is relatively well filled and not a sharp shell, we assume that its brightness distribution can be roughly approximated by an elliptical Gaussian with full width at 10% of peak of 49′ × 42′ (P.A. ~ 45°). Then, by choosing a nonthermal peak value and a background level on each map, it is possible to estimate its integrated flux density at 11, 6, and 3 cm. These are listed in Table 6. This Gaussian fitting technique, while only approximate, has the advantage of discriminating against the sharp emission peaks of the prominent H II regions near the southern edge of G8.7−0.1 in the short centimeter wavelength maps and providing a reasonable estimate of the integrated nonthermal emission. Very critical to the integrated flux density estimates are the assumed background levels so that they have been tabulated explicitly in Table 6 (col [3]). Determination of the background level is the dominant source of error, so that error estimates have been made by assuming a 50% deviation in the adopted background level.

At 90 cm, we estimate the SNR flux density of ~129 ± 11 Jy listed in Table 6 by measuring the total integrated flux density for the entire W30 complex (~146 Jy) and subtracting the contributions from the superposed H II regions B–G listed in Table 2 (~17 Jy). As can be seen, the thermal contribution is small and constitutes less than 15% of the 90 cm emission from the complex.

As mentioned above, 129 Jy may still be an underestimate if G8.7−0.1 is even larger than our 90 cm measurements can indicate. An independent estimate the flux of G8.7−0.1 near 90 cm is from the 408 MHz single-dish map of the region by Haslam *et al.* (1982). Their map, with a resolution of 0°85, shows a nearly unresolved source centered on the W30

© American Astronomical Society • Provided by the NASA Astrophysics Data System

1990ApJ...360..184K

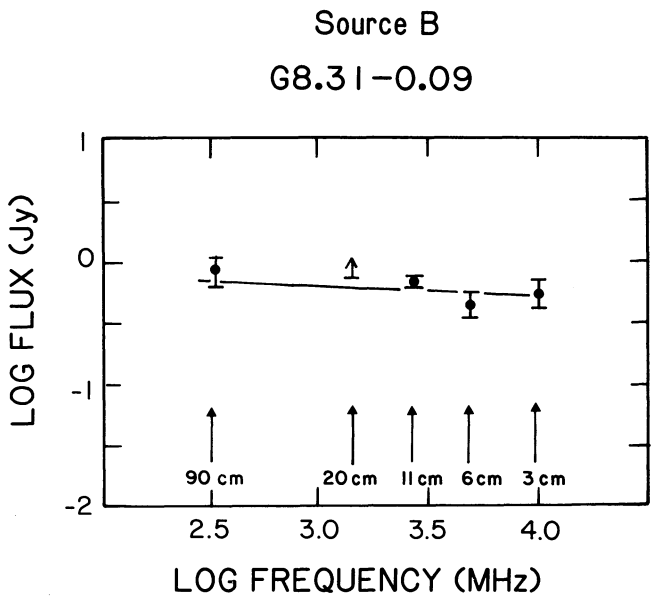

FIG. 6*a*

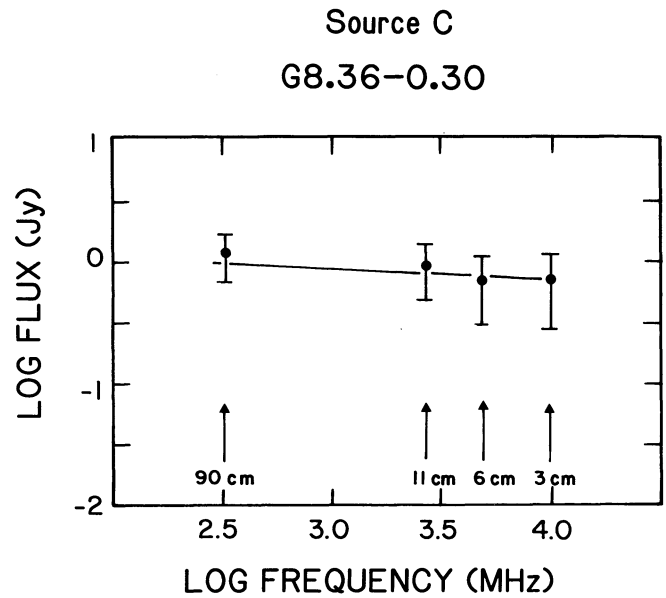

FIG. 6*b*

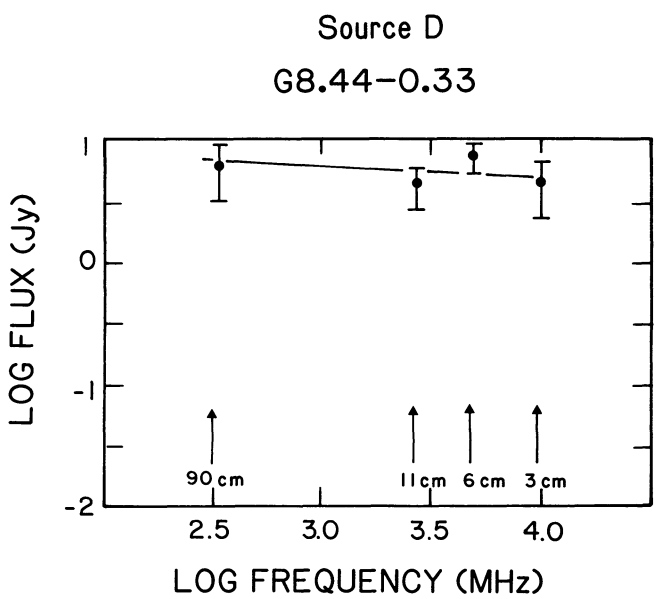

FIG. 6*c*

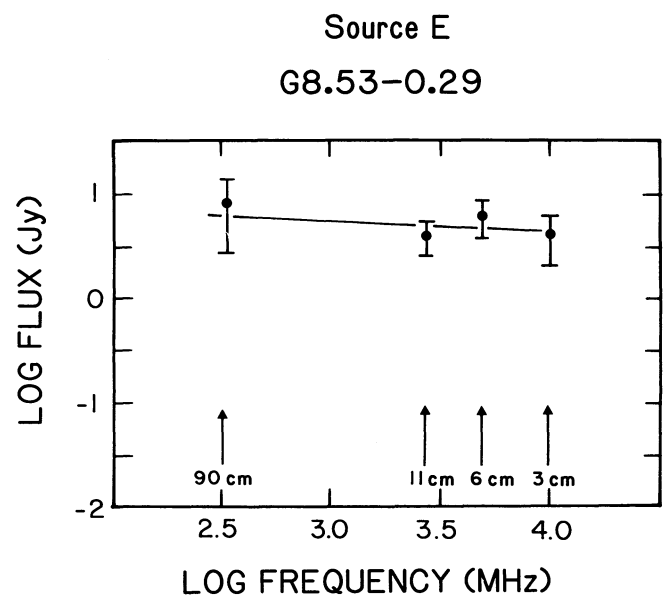

FIG. 6*d*

FIG. 6.—(*a*)–(*d*) Spectra of H II regions B–E in the W30 complex which are optically thin at 90 cm. Solid lines are straight spectra fitted to the measured 3, 6, and 11 cm flux densities listed in Table 4 and extrapolated to longer wavelengths with $\alpha = -0.1$. The available flux density measurements from Tables 2 and 4 are also plotted.

complex. Taking a Gaussian model with $T_{\rm peak} = 575$ K and $T_{\rm background} = 430 \pm 50$ K, their map gives $S_{408} \sim 165 \pm 50$ Jy. (A much older, lower resolution 408 MHz survey by Large, Mathewson, and Haslam 1961 lists a source at $l = 8\overset{\circ}{.}7$, $b = 0\overset{\circ}{.}0$ with an integrated flux density of 180 Jy, in good agreement with our estimate from the Haslam *et al.* 1982 map.) If ~ 20 Jy of the 408 MHz flux density is thermal emission then the flux density of G8.7−0.1 at 408 MHz is ~ 145 Jy. Extrapolating this value with a typical SNR spectrum of $\alpha = -0.5$ yields a 90 cm integrated flux density for G8.7−0.1 of ~ 160 Jy which is high but in reasonable agreement (to within the errors) with our measured value of ~ 130 Jy. Thus, if our 90 cm VLA observations are underestimating the flux density of G8.7−0.1, it is not likely to be more than by $\sim 30\%$. We list both the 330 and 408 MHz values in Table 6 and use them to determine the full spectrum for the SNR.

To estimate the flux density of G8.7−0.1 at 5 m (57.5 MHz) and 10 m (30.9 MHz) we assume that all the emission seen at such long wavelengths is nonthermal and use the integrated flux densities available in the literature (Odegard 1986*a*; Kassim 1988*a*, *b*). These are also listed in Table 6.

We fit the values listed in Table 6 with the equation:

$$S_\nu = [S_{408}(\nu/408)^\alpha] \exp\left[-\tau_{30.9}(\nu/30.9)^{-2.1}\right], \qquad (6)$$

where S_ν is the integrated flux density in Jy at frequency ν in

© American Astronomical Society • Provided by the NASA Astrophysics Data System

1990ApJ...360..184K

TABLE 6

INTEGRATED FLUX DENSITY ESTIMATES FOR G8.7−0.1

Wavelength (1)	Peak Brightness (K) (2)	Background Brightness (K) (3)	Integrated Flux Density (Jy) (4)	Size (maj × min) (5)	References (6)
3 cm	0.30	0.15	24.1 ± 12.0	49′ × 42′	Handa *et al.* 1988
6 cm	1.7	0.9	30.4 ± 17.1	...	Altenhoff *et al.* 1978
11 cm	6.3	3.0	36.7 ± 16.9	...	Reich *et al.* 1978
73.5 cm	575	430 ± 40	145 ± 45[a]	...	Haslam *et al.* 1982
90 cm	1166	...	≥129[b] ± 11	...	Present work
5 m	2.5×10^4	...	190 ± 50	...	Odegard 1986*a*
10 m	2.0×10^4	...	67 ± 13	...	Kassim 1988*a*

[a] Estimated from the 408 MHz single-dish map made by Haslam *et al.* 1982 with ∼0°.85 resolution. We have subtracted 20 Jy for the contributions from the superposed H II regions B–G.

[b] Corrected for the contribution (∼17 Jy) of superposed H II regions B–G (see Table 4, col. [2] and text).

MHz, S_{408} is the flux density at a reference frequency chosen to be 408 MHz and $\tau_{30.9}$ is the optical depth at 30.9 MHz. The intrinsic spectral index (α) of the SNR is assumed to be constant throughout the radio range (as appears to be true in general for SNRs; Kassim 1989), and $\tau_{30.9}$ is assumed to be due to free-free absorption along the line of sight averaged over the source. A least-squares fit to the available flux densities then yields $S_{408} = 120$ Jy, $\alpha = -0.5$, and $\tau_{30.9} = 2.0$. This derived spectrum is plotted as the solid line in Figure 7 along with the data points from Table 6.

The spectrum shown in Figure 7 is typical for SNRs located toward the inner Galaxy since low-frequency turnovers are relatively common (Dulk and Slee 1972, 1975; Kassim 1987, 1989). Also, the high-frequency spectral index of $\alpha = -0.5$ is typical for shell-type SNRs (Clark and Caswell 1976). The index of $\alpha = -0.25$ derived by Odegard (1986*a*) is too flat because of absorption by H II regions along the line of sight of his 57.5 MHz observations.

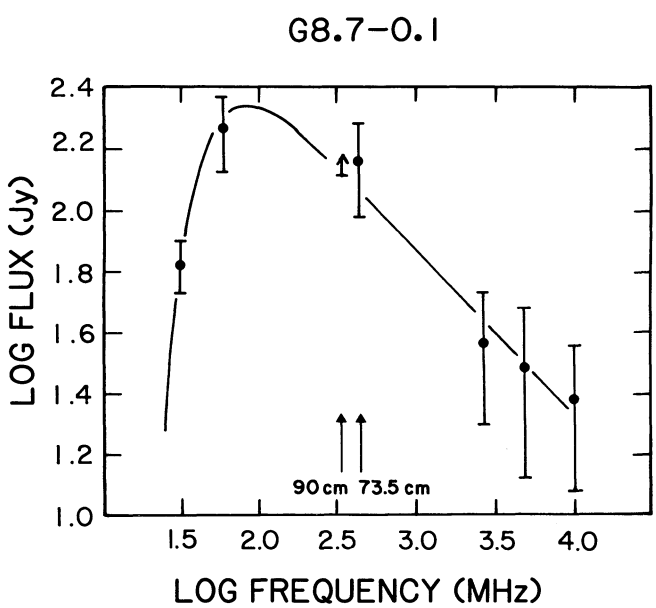

FIG. 7.—Spectrum for G8.7−0.1. The low-frequency turnover shown here is typical for Galactic SNRs in the inner Galaxy (Kassim 1989), and is due to absorption by ionized gas associated with foreground H II regions along the line of sight.

ii) *Spectral Turnover*

In his extensive study of the spectra of Galactic SNRs, Kassim (1987, 1989, and references therein) has shown that low-frequency (<100 MHz) turnovers are due to free-free absorption by intervening ionized gas, probably associated with normal H II regions or their low-density halos superposed along the line of sight, rather than absorption by a distributed ionized component of the ISM. He found that such absorption is patchy and even some distant SNRs, show no spectral turnovers down to the lowest available frequencies.

In G8.7−0.1, we have an example of an SNR with a spectral turnover where the patchiness of the absorbing regions can actually be observed. Moreover, $\tau_{30.9} = 2.0$, a spatial average over a patchy absorbing screen, it typical of the values found by Kassim (1989).

V. DISTANCES TO SOURCES IN THE W30 COMPLEX

a) Distances to the H II *Regions*

Distances to H II regions are usually derived kinematically from recombination line velocities and a model for Galactic rotation. This often leads to a twofold ambiguity with "near" and "far" kinematic distances. Occasionally this ambiguity can be resolved by complimentary observations of H I or H_2CO absorption spectra toward the source of interest.

In the W30 complex, sources A–G have radio recombination line detections (see Table 3) and the distance ambiguity has been resolved for sources C and F. Downes *et al.* (1980) list a distance of 6 ± 1 kpc for both sources from H110α recombination line observations combined with complementary formaldehyde absorption measurements.[6] Fortunately, the measured recombination line velocities for sources B, D, E, and G are all within ∼5 km s^{-1} of that for sources C and F at ∼40 km s^{-1} so that it is a reasonable assumption that each of the five sources B–F is associated with the same complex near 6 kpc. Source A lies outside of the W30 complex and with a recombination line velocity of ∼20 km s^{-1} is probably not associated with W30.

[6] Downes *et al.* (1980) also list distances to sources C and F of 5.5 and 5.3 kpc, respectively, as determined from earlier studies by Wilson (1972) (for source C) and Georgelin and Georgelin (1976) (for source F). Both distance estimates are consistent, within the errors, of the Downes *et al.* estimate of 6 ± 1 kpc. All distances are based on assuming D_{GC} for the Sun of 10 kpc and the Schmidt model for Galactic rotation.

© American Astronomical Society • Provided by the NASA Astrophysics Data System

1990ApJ...360..184K

Another method to resolve the distance ambiguity for thermal sources in the Galactic plane is to use very low frequency continuum measurements. H II regions which are large and foreground can be seen in absorption against the Galactic or other nonthermal background, whereas far (or small compared to the beam) H II regions will be undetected at low frequencies. Thus the extended H II regions C and D (see § IV*a*) which are seen as strong absorption features on the 57.5 MHz map of Odegard (1986*a*) (Fig. 4) must be at the near kinematic distance of ~6 kpc rather than the far at ~14 kpc. This is in agreement with radial velocity arguments given above which place sources B–F at ~6 kpc. The fact that sources F and G do not appear as absorbers at 57.5 MHz is not disturbing. They are known to be small (Table 4) with respect to the 57.5 MHz beam, and their absorption would be diluted to undetectable levels.

With a distance established for the H II regions B–G, it is possible to estimate (or place a limit on) their physical sizes and these are listed in Table 7.

b) *Constraints on the Distance to G8.7−0.1*

It is possible to establish a distance estimate to G8.7−0.1 independent of the traditional (and mistrusted) Σ–*D* (surface brightness–linear diameter) relation by (1) relating G8.7−0.1 to the H II regions in the W30 complex, and (2) using OH absorption spectra from the literature.

i) *A Relation between G8.7−0.1 and the W30* H II *Regions*

Since H II regions C and D are seen in absorption against G8.7−0.1 at 57.5 MHz (see Fig. 4), they almost certainly lie in front of it and thus place the SNR at ≥6 kpc. In addition, thermal source E is not seen in absorption at 57.5 MHz even though we have good evidence that it is extended (see Figs 2 and 3 and Table 4), so that it is apparently behind G8.7−0.1. Thus, we can also set an upper limit to the distance to G8.7−0.1 of ≤6 kpc. With the caveat that this upper limit to the distance is less firm than the lower limit (since *not* seeing an absorption is more difficult to be certain of than actually seeing an absorption and the W30 region is very complex within the 57.5 MHz resolution), G8.7−0.1 appears to be one of the few (see, e.g., Green 1984) SNRs where an independent distance estimate can be established. Allowing for error in the H II region distance estimates, we take the distance of G8.7−0.1 to be 6 ± 1 kpc. The relationship between G8.7−0.1 and the W30 H II regions is summarized in column (4) of Table 7.

It should also be noted that although the upper limit on the distance to G8.7−0.1 is weaker, the SNR cannot be much more distant. At ~6 kpc, it is already one of the physically largest and lowest surface brightness SNRs known (see § VI). Note also that ~6 kpc is 2–3 times more distant than was estimated by Odegard (1986*a*) from the Σ–*D* relation for SNRs, but still lies within the expected errors of that rather uncertain relationship (see, e.g., Green 1984).

ii) *Lower Distance Limit to G8.7−0.1 from OH Absorption Spectra*

A second means for estimating the distance to G8.7−0.1 is from OH absorption spectra. The Galactic survey by Turner (1979) samples several regions in the W30 complex with a spatial resolution of ~18′. Two strong absorption features near 17 and 38 km s^{-1} are clearly detected for numerous positions, several of which are in directions where the telescope beam contains at least one of the known ~40 km s^{-1} recombination line velocity H II regions. Such an H II region in the beam can provide the background continuum emission against which the OH absorption is seen. However, a measurement at $\alpha = 18^h02^m47^s.1$, $\delta = -21°25'19''$ still shows both the 17 and 38 km s^{-1} absorption features but has no known thermal emission regions within the beam. (The nearest H II region is more than 20′ from the beam center.) Since the OH absorption position is centered near the peak brightness of G8.7−0.1 on our 90 cm map, it is reasonable to assume that this absorption is being seen against the nonthermal emission from the SNR. Thus, the OH absorption also implies a lower limit to the distance of G8.7−0.1 which is comparable to that for the W30 H II regions, i.e., ~6 kpc.

VI. PHYSICAL PROPERTIES OF G8.7−0.1

With a reliable distance (§§ V*b*[i] and V*b*[ii]) and spectrum (§ IV*b*[ii]) available, it is possible to estimate the physical properties of G8.7−0.1, and these are given in Table 8. Most values are typical for Galactic SNRs. A spectral index of $\alpha = -0.5$ is average (Clark and Caswell 1976) for shell-type SNRs, and the absolute luminosity at 1 GHz of ~2400 Jy kpc^2 is well within the large range of values known for other SNRs. Of 10 SNRs with good distance estimates (Green 1984), the average luminosity at 1 GHz is ~4500 Jy kpc^2 but with a wide scatter ($\sigma \sim 6000$ Jy kpc^2) due mainly to the unusually high luminosity of ~21,000 Jy kpc^2 for Cas A. Excluding Cas A from the calculations brings G8.7−0.1 quite close to the average luminosity of ~2800 Jy kpc^2. Its angular extent of ~45′, however, implies a linear size of ~80 pc, making G8.7−0.1 marginally the largest of any known Galactic SNR with a well-determined distance. Only HB3 (size ~ 70 pc) and Kes 67 (size ~75 pc) are of comparable size. Adding G8.7−0.1 to the traditional surface brightness-linear diameter (Σ–*D*) plot for SNRs (Fig. 8) does little to either strengthen or weaken the arguments surrounding this controversial relationship. However, Figure 8 does emphasize that G8.7−0.1 is one of the

TABLE 7

PHYSICAL SIZES OF H II REGIONS IN THE W30 COMPLEX[a]

Source	Angular Size[b] (arcmin)	Physical Size (pc)	Position Relative to G8.7−0.1
B	≤1.0 × 0.5	≤0.7	Unknown
C	≤2.7 × 2.7	≤2.4	Foreground
D	8.5 × 8.5	14.8	Foreground
E	9.2 × 7.1	14.2	Background
F	≤1.8 × 0.9	≤2.4	Unknown
G	≤1.8 × 0.9	≤2.4	Unknown

[a] All objects are at 6 ± 1 kpc (see § V*a*), and $D_{GC} = 10$ kpc for the Sun is assumed.

[b] From Table 4.

TABLE 8

MEASURED AND DERIVED PROPERTIES FOR G8.7−0.1

Parameter	Value
Spectral index	−0.53 ($S \propto \nu^{+\alpha}$)
Σ(1 GHz)	5.7×10^{-21} W m^{-2} Hz^{-1} sr^{-1}
Distance[a]	6 ± 1 kpc
Absolute Luminosity (@ 1 GHz)	2758 Jy kpc^2
Angular size	49′ × 42′ (P.A. ~45°)
Linear diameter	~79 pc

[a] Based on assuming $D_{GC} = 10$ kpc for the Sun.

© American Astronomical Society • Provided by the NASA Astrophysics Data System

1990ApJ...360..184K

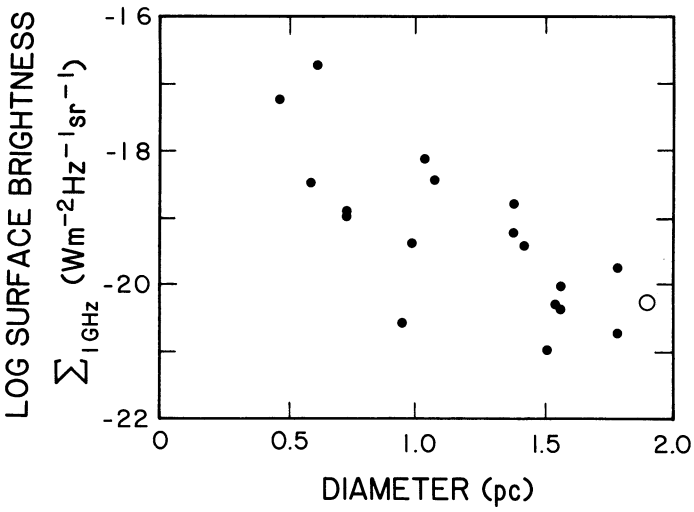

FIG. 8.—The position of G8.7−0.1 (represented by a circled cross) on the standard surface brightness vs. linear diameter (Σ–D) plot. The units of surface brightness are W m^{-2} Hz^{-1} sr^{-1}. Data for all sources except G8.7−0.1 have been taken from Green (1984, 1988*a*). This plot shows that G8.7−0.1 is one of the physically largest and lowest surface brightness SNRs known in our Galaxy.

physically largest and lowest surface brightness Galactic SNRs presently known.

VII. A POSSIBLE RELATION BETWEEN G8.7−0.1 AND PSR 1800−21

PSR 1800−21 is unusually young ($\sim 1.6 \times 10^4$ yr) and fast (P = 133.6 ms) (Clifton and Lyne 1986). Its position has been determined to high accuracy by the VLA A-array and single-dish timing observations (Braun, Goss, and Lyne 1989). It is included in our 90 cm field of view but is not detected to a flux density limit of less than 0.25 Jy (Table 2). This upper limit at 90 cm combined with a 20 cm detection of $\sim$15 mJy by Braun, Goss, and Lyne (1989) implies a spectral index $\alpha > \sim -2$ (where $S \propto \nu^{+\alpha}$).

Examination of Figure 1 (pulsar position marked with a star) shows that PSR 1800−21 appears to lie within the western extent of G8.7−0.1 at 90 cm. Since very few pulsar–SNR connections are well established, the possibility of an association is intriguing. This is especially true since PSR 1800−21 is estimated to be $\sim$17,000 years old and at a distance of $\sim$5.3 kpc (Clifton and Lyne 1986). Odegard (1986*a*) has used a surface brightness age (Σ–t) relation to estimate an age of $\sim$15,000 years for G8.7−0.1 which, if true, makes it one of the youngest SNRs known and of similar age to PSR 1800−21. Combined with our distance estimate (§ V*b*) of $\sim$6 kpc, this makes PSR 1800−21 and G8.7−0.1 likely to be related in space and physically as well as in projection on the sky. However, if the position of a supernova leading to the creation of both G8.7−0.1 and PSR 1800−21 were near the center of the 90 cm SNR emission seen in Fig. 1 and it exploded only $\sim$15,000–20,000 years ago, the required transverse velocity of PSR 1800−21 to reach its present position near the edge of G8.7−0.1 is extremely high, $\sim$1700 km s^{-1}. These issues are sufficiently complex that they are discussed in more detail elsewhere (Kassim and Weiler 1990).

VIII. CONCLUSIONS

We have used the VLA to observe the W30 H II/SNR complex at 90 and 20 cm wavelength. By combining these observations with higher frequency centimeter wavelength single-dish observations and lower frequency meter wavelength interferometer observations we have been able to estimate spectra for each of the known thermal sources. For the H II regions which are optically thin at 90 cm we have derived upper limits to their emission measures, and for those which are optically thick we have set lower limits to both their emission measures and filling factors. The results are consistent with the expectation that H II regions with compact ($\sim < 1'$) structure become optically thick at higher frequencies than those with more extended structure. Thus, our 90 cm VLA observations provide a method for easily screening thermal sources for compact structure.

From this derived knowledge of the thermal sources, we are able to establish the relative contributions of thermal and nonthermal emission in the W30 complex and to obtain improved estimates of the spectrum and morphology of the W30 SNR, G8.7−0.1. Our new 90 cm observations show that the SNR is larger and has a steeper spectrum ($\alpha \sim -0.5$) than previously realized. The spectrum of G8.7−0.1 is also shown to turn over below $\sim$100 MHz, a form typical of the low-frequency spectra of many Galactic SNRs located toward the inner Galaxy. The G8.7−0.1 spectral turnover is consistent with absorption by localized gas associated with thermal sources near the W30 complex and does not require absorption by a distributed ionized component of the ISM.

We have also been able to use the rather well established distance estimates to H II regions in W30 to constrain the distance to G8.7−0.1. A number of the H II regions in the complex go into absorption against the SNR at meter wavelengths, showing that G8.7−0.1 is behind them or at greater than $\sim$6 kpc. This distance estimate is also supported by previously published OH absorption spectra against the SNR and H II regions. A somewhat weaker argument involving the lack of detectable absorption for one H II region in W30 implies that G8.7−0.1 is also at less than $\sim$6 kpc, placing the SNR at 6 ± 1 kpc.

At this distance, G8.7−0.1 is one of the largest known Galactic SNRs, with a physical size of $\sim$80 pc, and certainly one of the most distant, low–surface brightness members of the class. It is well known that current SNR catalogs strongly select against such objects (Green 1984, 1988*a*, *b*) so that low-frequency observations appear to offer probably the best chance of reducing this incompleteness.

Our distance estimate to G8.7−0.1 also places it close in space to the recently discovered young, fast pulsar PSR 1800−21. They also appear to have similar ages 15,000–20,000 years. While dynamical problems remain in establishing a physical SNR/PSR association, possibility of a connection is sufficiently intriguing that it is outlined here and discussed in more detail elsewhere (Kassim and Weiler 1990).

Finally, the authors would like to thank the refree for several useful comments which have been incorporated into the manuscript.

© American Astronomical Society • Provided by the NASA Astrophysics Data System

1990ApJ...360..184K

REFERENCES

Altenhoff, W. J., Downes, D., Pauls, T., and Schraml, J. 1978, *Astr. Ap., Suppl.*, **35**, 23.
Blitz, L., Fich, M., and Stark, A. A. 1982, *Ap. J. Suppl.*, **49**, 183.
Braun, R., Goss, W. M., and Lyne, A. G. 1989, *Ap. J.*, **340**, 355.
Clark, D. H., and Caswell, J. L. 1976, *M.N.R.A.S.*, **174**, 267.
Clifton, T. R., and Lyne, A. G. 1986, *Nature*, **320**, 43.
Downes, D., Wilson, T. L., Bieging, J., and Wink, J. 1980, *Astr. Ap. Suppl.*, **40**, 379.
Dulk, G. A., and Slee, O. B. 1972, *Australian J. Phys.*, **25**, 429.
———. 1975, *Ap. J.*, **199**, 61.
Erickson, W. C. 1983, *Ap. J. (Letters)*, **264**, L13.
Erickson, W. C., Mahoney, M. J., and Erb, K. 1982, *Ap. J. Suppl.*, **50**, 403.
Garwood, R. W., Perley, R. A., Dickey, J. M., and Murray, M. A. 1988, *A.J.*, **96**, 1655.
Georgelin, Y. M., and Georgelin, Y. P. 1976, *Astr. Ap.*, **49**, 57.
Green, D. A. 1984, *M.N.R.A.S.*, **209**, 449.
———. 1988*a*, *Ap. Space Sci.*, **148**, 3.
———. 1988*b*, in *Lecture Notes in Physics*, Vol. **316**, *Supernova Shells and Their Birth Events*, ed. W. Kundt (Berlin: Springer), pp. 39–43.
Handa, T., Sofue, Y., Naomasa, N., Hirabayashi, H., and Inoue, M. 1988, *Pub. Astr. Soc. Japan*, **39**, 709.
Haslam, C. G. T., Salter, C. J., Stoffel, H., and Wilson, W. E. 1982, *Astr. Ap. Suppl.*, **47**, 1.
Hjellming, R. M., Andrews, M. H., and Sejnowski, T. J. 1969, *Ap. J.*, **157**, 573.
Kassim, N. E. 1987, Ph.D. thesis, University of Maryland.
———. 1988*a*, *Ap. J. (Letters)*, **328**, L55.
Kassim, N. E. 1988*b*, *Ap. J. Suppl.*, **68**, 715.
———. 1989, *Ap. J.*, **347**, 915.
Kassim, N. E., and Weiler, K. W. 1990, *Nature*, **343**, 146.
Kassim, N. E., Weiler, K. W., Erickson, W. C., and Wilson, T. L. 1989, *Ap. J.*, **338**, 152 (K89).
Large, M. I., Mathewson, D. S., and Haslam, C. G. T. 1962, *M.N.R.A.S.*, **123**, 113.
Lockman, F. J. 1989, *Ap. J. Suppl.*, **71**, 469.
Mezger, P. G., and Henderson, A. P. 1967, *Ap. J.*, **147**, 471.
Napier, P. J., Thompson, A. R., and Ekers, R. D. 1983, *Proc. IEEE*, **71**, 1295.
Odegard, N. 1986*a*, *A.J.*, **92**, 1372.
———. 1986*b*, *Ap. J.*, **301**, 813.
Reich, W., Furst, E., Steffen, P., Reif, K., and Haslam, C. G. T. 1984, *Astr. Ap. Suppl.*, **58**, 197.
Seaton, M. J. 1980, in *Radio Recombination Lines*, ed. P. A. Shaver (Dordrecht: Reidel), p. 3.
Shaver, P. A. 1980, *Astr. Ap.*, **91**, 279.
Turner, B. E. 1979, *Astr. Ap. Suppl.*, **37**, 1.
Wilson, T. L. 1972, *Astr. Ap.*, **19**, 354.
———. 1980, in *Radio Recombination Lines*, ed. P. A. Shaver (Dordrecht: Reidel), p. 205.
Wink, J. E., Wilson, T. L., and Bieging, J. H. 1983, *Astr. Ap.*, **127**, 211.
Wood, D. O. S., and Churchwell, E. 1989, *Ap. J. Suppl.*, **69**, 831.
Wood, D. O. S., Handa, T., Fukui, Y., Churchwell, E., Sofue, Y., and Iwata, T. 1988, *Ap. J.*, **326**, 884.

NAMIR E. KASSIM and KURT W. WEILER: NRL-Code 4030, Washington, DC 20375-5000

© American Astronomical Society • Provided by the NASA Astrophysics Data System